

A propeller scenario for the gamma-ray emission of low-mass X-ray binaries: The case of XSS J12270–4859

A. Papitto^{1*}, D. F. Torres^{1,2}, Jian Li¹

¹*Institute of Space Sciences (IEEC-CSIC), Campus UAB, Fac. de Ciències, Torre C5, parell, 2a planta, 08193 Barcelona, Spain*

²*Institució Catalana de Recerca i Estudis Avançats (ICREA), 08010 Barcelona, Spain*

23 October 2021

ABSTRACT

XSS J12270–4859 is the only low mass X-ray binary (LMXB) with a proposed persistent gamma-ray counterpart in the *Fermi*-LAT domain, 2FGL 1227.7–4853. Here, we present the results of the analysis of recent INTEGRAL observations, aimed at assessing the long-term variability of the hard X-ray emission, and thus the stability of the accretion state. We confirm that the source behaves as a persistent hard X-ray emitter between 2003 and 2012. We propose that XSS J12270–4859 hosts a neutron star in a propeller state, a state we investigate in detail, developing a theoretical model to reproduce the associated X-ray and gamma-ray properties. This model can be understood as being of a more general nature, representing a viable alternative by which LMXBs can appear as gamma-ray sources. In particular, this may apply to the case of millisecond pulsars performing a transition from a state powered by the rotation of their magnetic field, to a state powered by matter in-fall, such as that recently observed from the transitional pulsar PSR J1023+0038. While the surface magnetic field of a typical NS in a LMXB is lower by more than four orders of magnitude than the much more intense fields of neutron stars accompanying high-mass binaries, the radius at which the matter in-flow is truncated in a NS-LMXB system is much lower. The magnetic field at the magnetospheric interface is then orders of magnitude larger at this interface, and as consequence, so is the power to accelerate electrons. We demonstrate that the cooling of the accelerated electron population takes place mainly through synchrotron interaction with the magnetic field permeating the interface, and through inverse Compton losses due to the interaction between the electrons and the synchrotron photons they emit. We found that self-synchrotron Compton processes can explain the high energy phenomenology of XSS J12270–4859.

Key words: acceleration of particles – accretion, accretion discs – magnetic fields – X-rays: individual: – gamma-rays: stars

1 INTRODUCTION

When captured by the gravitation of a neutron star, the interaction between the matter outflow coming from a companion star (such as the Be decretion disc of a Be star, or the Roche Lobe overflowing matter from a low mass star) and the magnetic field of a neutron star can lead to several states. A pulsar (ejector), a propeller, or an accretion state can be realised depending on the balance between the pressure exerted by the inflowing matter and by the rotating magnetic field of the neutron star (see, e.g. Lipunov et al. 1992, for a review). When the mass in-flow is able to bound the magnetosphere to a closed configuration, whether accretion down to the neutron star surface is possible (accretor state) or mass is propelled away by the neutron star magnetosphere (propeller state) is mainly determined by the ratio between the rotation rate of the

magnetosphere and of the incoming matter at the magnetospheric boundary (Illarionov & Sunyaev 1975). At such interface, in some cases the magnetosphere yields energy and angular momentum to the matter inflow, and the plasma is expected to be very turbulent and magnetised. Bednarek (2009a,b) argued how in such conditions electrons can be accelerated to high energies by a Fermi process, yielding a detectable emission at GeV and TeV energies. In a similar context, Torres et al. (2012) explained the seemingly anti-correlated orbital variability of the GeV and TeV emission of LS +61° 303 in terms of the alternation between the propeller and the ejector state of a magnetised neutron star, as the neutron star experiences different mass in-flow rates along its orbit.

Here, we propose a propeller scenario to explain the properties of the high energy emission of XSS J12270–4859, so far the only low-mass X-ray binary (LMXB) proposed to have a persistent gamma-ray counterpart, actually emitting a comparable power in X-rays and at HE, 2FGL 1227.7–4853 (De Martino et al. 2010;

* E-mail: papitto@ice.csic.es

Hill et al. 2011; De Martino et al. 2013). Unlike gamma-ray binaries, in this case both the wind and the radiative output of the low mass companion star are unimportant in determining the HE emission properties. Instead, we propose a model in which electrons are accelerated at the interface between an accretion disc and a propelling neutron star, and which losses are mainly driven by synchrotron emission. Indeed, this electron population interacts with the magnetic field permeating such layer and with the radiation thus produced to yield the X-ray and GeV emission observed from the source.

The paper is organised as follows. In Sec. 2 we review the properties of XSS J12270–4859 and of its proposed γ -ray counterpart, 2FGL 1227.7–4853. In Sec. 3 we present the results of the analysis of recent INTEGRAL observations, aimed at assessing the long-term variability of the hard X-ray emission, and thus the stability of the accretion state. In Sec. 4 we derive expressions relating the observed luminosity to the relevant physical parameters of the system, spin period, magnetic field, and mass inflow rate, under the assumption that it hosts a propelling neutron star with typical parameters of LMXBs. In Sec. 5 we reproduce semi-quantitatively the high energy spectral energy distribution produced by a relativistic population of electrons located at the boundary between an accretion disc and a propelling magnetosphere, under simple assumptions on the shape of the emitting region. We discuss these results in Sec. 6, comparing our scenario with other possible models proposed to explain the system, involving either a rotation powered pulsar or an accreting compact object.

2 XSS J12270–4859

XSS J12270–4859 is a faint hard X-ray source, first identified as a Cataclysmic Variable on the basis of its optical spectrum (Masetti et al. 2006). However, the absence of a clear modulation of the emission in the X-ray (Saitou et al. 2009; De Martino et al. 2010) and in the optical bands (Pretorius 2009), as well as the absence of Fe K- α features in X-rays, forced to disregard such hypothesis.

XSS J12270–4859 was observed on several occasions in the X-ray band: by RXTE in November 2007 and during 2011 (3–60 keV; Butters et al. 2008; De Martino et al. 2013), by XMM-Newton in January 2009 and January 2011 (0.5–10 keV; De Martino et al. 2010, 2013), by Suzaku in August 2009 (0.2–12 and 10–600 keV; Saitou et al. 2009), by Swift/XRT between March and September 2011 (0.5–10 keV De Martino et al. 2013), and by INTEGRAL since March 2003 (20–100 keV; see De Martino et al. 2010, who reported the analysis up to October 2007). Its average 0.2–100 keV luminosity was evaluated by De Martino et al. (2010) as $L_X = (2.2 \pm 0.4) \times 10^{34} d_2^2 \text{ erg s}^{-1}$, where d_2 is the distance in units of 2 kpc. Its spectrum is described by a featureless power law, $F_E \propto E^{-(\Gamma_X-1)}$, with an index $\Gamma_X = 1.70 \pm 0.02$, without any detected cut-off up to 100 keV (Saitou et al. 2009; De Martino et al. 2010, 2013). The light curve below 10 keV shows peculiar dips and flares on time scales of few hundreds of seconds, suggesting an accretion nature of the X-ray emission (Saitou et al. 2009; De Martino et al. 2010, 2013). Flares are followed by dips in which a spectral hardening is observed, suggestive of additional absorption by a flow of cool matter. Dips with little to none spectral evolution also occur randomly during the quiescent emission, and are possibly interpreted in terms of occultation by discrete blobs of material.

The emission of the IR/optical/UV counterpart is compati-

ble with the sum of the thermal emission of a K2-K5 V star at a distance of 2.3–3.6 kpc, and of a hotter thermal emission coming from a surface of larger size, compatible with an accretion disc (De Martino et al. 2013). Dips and flares take place almost simultaneously in the UV and X-ray band; together with the observed relative amplitudes of the flares in these two bands, this strongly indicates that the UV emission originate from reprocessing of the X-emission in a larger region than where the higher energy emission is generated (De Martino et al. 2013). The presence of material around the compact object is further indicated by the detection of several emission lines typical of accreting systems, such as H α , H β and HeII, (Masetti et al. 2006; Pretorius 2009), as well as by an optical spectrum recently obtained by NTT during March 2012 (De Martino 2013, priv. comm.).

XSS J12270–4859 is positionally coincident with a moderately bright gamma-ray source detected by *Fermi*-LAT, 2FGL 1227.7–4853 (De Martino et al. 2010; Hill et al. 2011; De Martino et al. 2013). *Fermi*-LAT observations performed between August 2008 and September 2010 revealed a source with spectrum described by a power law with index 2.21 ± 0.09 , cut off at $\Gamma_\gamma = 4.1 \pm 1.3$ GeV, and with a luminosity of $L_\gamma = (2.3 \pm 0.3) \times 34 d_2^2 \text{ erg s}^{-1} \simeq L_X$ above 100 MeV (Hill et al. 2011)¹. These authors also discussed the possible association of 2FGL 1227.7–4853 with two radio sources detected by ATCA at 5.5 and 9 GHz, falling in its error circle. They identified the radio counterpart of XSS J12270–4859 (a faint source with a $F_\nu \propto \nu^{-\alpha}$ power-law spectrum, with $\alpha = 0.5 \pm 0.6$) as the least improbable association, given the extremely low radio-to-gamma ray luminosity ratio shown by the other one, most probably an AGN. No significant variation of the gamma-ray emission of the source were found by De Martino et al. (2013), who extended the analysis including data taken until April 2012. Their analysis also proved that the gamma-ray emission is concurrent with observations performed at soft (XMM-Newton, Suzaku, Swift/XRT) and hard (RXTE) X-rays.

3 INTEGRAL OBSERVATIONS OF XSS J12270–4859

De Martino et al. (2010) reported the analysis of *INTEGRAL*/ISGRI observations of XSS J12270–4859 performed between March 2003 and October 2007, and used them together with RXTE and XMM-Newton observations to build a 0.2–100 keV spectrum which was successfully modelled by a power-law with index $\Gamma_X = 1.70 \pm 0.02$. In order to study the long-term variability of the hard X-ray emission of XSS J12270–4859, and to analyse *INTEGRAL* observations simultaneous to those *Fermi*-LAT observations reported by Hill et al. (2011) and performed between August 2008 and September 2009, we analysed all *INTEGRAL* (Winkler et al. 2003) observations performed from March 2003 to July 2012.

Observations performed by *INTEGRAL* are carried out in individual Science Window (ScW), which have a typical time duration of about 2 ks. Here, we consider all public IBIS/ISGRI and JEM-X observations during which XSS J12270–4859 has offset angle less than 14° and 5°, respectively, adding up to a total effective exposure time of 553.7 ks for IBIS/ISGRI and 39.1 ks for JEM-X (22.9 ks from JEM-X 1 and 16.2 ks from JEM-X 2). Data reduction was

¹ Here, only statistical errors are quoted. Systematic errors can be larger by a factor \sim three. See Hill et al. 2011 for a discussion of this issue.

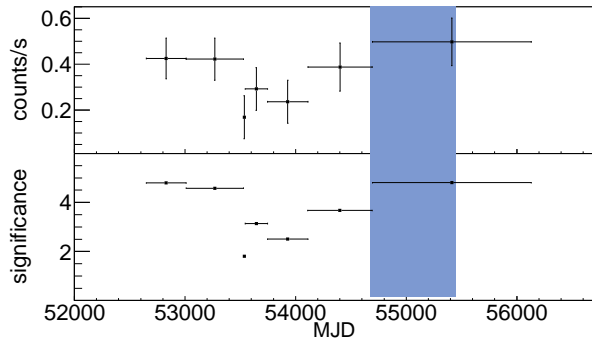


Figure 1. Long-term light curve (upper panel) and significance (lower panel) of XSS J12270–4859 on ScW timescales as seen by IBIS/ISGRI in the 18–60 keV band. The interval covered by *Fermi-LAT* data reported by Hill et al. (2011) is highlighted in blue. Here labels should be printed with a larger font size.

Table 1. Flux, detected significance and effective exposure time of 7 evenly divided time spans of ISGRI observations of XSS J12270–4859

Time covered (MJD)	Intensity (s^{-1})	Signif. (σ)	Expos. (ks)
52650.7 – 53010.2	0.42	4.79	79.2
53010.2 – 53528.3	0.42	4.58	78.9
53528.4 – 53543.5	0.17	1.81	80.1
53543.6 – 53746.9	0.29	3.14	79.3
53746.9 – 54110.9	0.24	2.50	79.2
54111.1 – 54692.7	0.39	3.67	79.6
54693.7 – 56131.0	0.50	4.80	79.1

performed using the standard ISDC offline scientific analysis software version 10.0.

While XSS J12270–4859 was not detected by JEM–X at a significance larger than 3σ , we confirm the previous INTEGRAL/ISGRI detection reported by De Martino et al. (2010). Combining all the ISGRI data, XSS J12270–4859 is detected at a significance level of 10σ in the 18–60 keV band, with an average count rate of $0.365 \pm 0.036 \text{ s}^{-1}$. Since XSS J12270–4859 itself is relatively faint in hard X-rays comparing to other sources in this region, the energy spectrum was obtained from the mosaic images. Its average spectrum can be described by a power law with index of 1.67 ± 0.27 , for a luminosity of $(8.8 \pm 0.1) \times 10^{33} \text{ d}_2^2 \text{ erg s}^{-1}$ in the 18–60 keV band, compatible with the value derived by De Martino et al. (2010) on a smaller data set. The reduced χ^2 for the fit is 0.6 under 3 d.o.f.

To study the long-term variability of the emission observed by ISGRI we divided the whole exposure into seven time intervals, each with an exposure of roughly 80 ks. The latter is the exposure – concurrent with *Fermi-LAT* observations – during which the source is found with a significance of 4.5σ . The light curve, significance and effective exposure for each time span are shown in Figure 1 and Table 1. The source is detected at a significance $\gtrsim 3\sigma$ in all but the third interval, which is the one covering the shorter time period (15 days), and during which the significance falls to 1.8σ . However, modelling the overall light curve with a constant gives a $\chi^2 = 9$ over six degrees of freedom, clearly indicating that the observed emission is compatible with a constant.

Finally, in order to search for any periodic signal in the long-

term light curve, we use the Lomb–Scargle periodogram method (Lomb 1976; Scargle 1982). Power spectra are generated for the light curve using the PERIOD subroutine (Press et al. 1989). The 99% white noise significance levels are estimated using Monte Carlo simulations (see e.g. Kong et al. 1998). No signal was significantly detected beyond such noise level.

Our analysis indicates that XSS J12270–4859 keeps behaving as a steady hard X-ray emitter, over a 9-year time interval. Also, it shows that the source was active in hard X-rays simultaneously to the *Fermi* observations performed between August 2008 and September 2010 and analysed by Hill et al. (2011), confirming the simultaneous RXTE/*Fermi* detection achieved during 2011 (De Martino et al. 2013).

4 PROPELLER STATE

The fate of matter in-falling towards a magnetised rotating neutron star depends essentially on the ratio between the rotation rate of the in-flowing matter and of the magnetosphere, evaluated at the radius where the dynamics of the flow becomes dominated by the stress exerted by the magnetic field, the so-called disk truncation radius R_{in} (see, e.g. Ghosh 2007, and references therein). In a Keplerian this disk, matter rotates at a rate:

$$\Omega_{\text{K}}(r) = (GM_*/r^3)^{1/2}, \quad (1)$$

where M_* is the mass of the compact object, and it is useful to define the fastness parameter as the ratio between the neutron star rotation rate, $\Omega_* = 2\pi/P$, and the Keplerian rate at the truncation radius:

$$\omega_* = \frac{\Omega_*}{\Omega_{\text{K}}(R_{\text{in}})} = \left(\frac{R_{\text{in}}}{R_{\text{c}}}\right)^{3/2}. \quad (2)$$

Here

$$R_{\text{c}} = (GM_*/\Omega_*^2)^{1/3} \quad (3)$$

is the co-rotation radius. While for $\omega_* < 1$ (*slow rotator case*), mass in the disc is allowed to accrete yielding its specific angular momentum to the neutron star, for $\omega_* \geq 1$ (*fast rotator case*), the in-flowing mass finds a centrifugal barrier which partly or completely inhibit further in-fall onto the surface of the neutron star.

Such a bi-modality of the outcome of accretion follows from the nature of the coupling between the field lines and the disc matter. In order to flow towards the compact object in a Keplerian disk at a steady rate \dot{M} , matter has to get rid of its angular momentum at a rate:

$$(d/dt)L_{\dot{M}}(r) = \dot{M}\Omega_{\text{K}}(r)r^2. \quad (4)$$

Far from the central object, it is disk viscosity which redistributes this angular momentum towards the outer rings of the disk. As matter approaches a magnetised neutron star, the stress exerted by its rotating magnetic field becomes dominant. Differential rotation between the field lines, assumed to be initially poloidal, and disk matter yields a stress:

$$S^{\text{m}} = \pm B_p B_\phi / 4\pi, \quad (5)$$

where B_ϕ is the toroidal component of the field originated from the twisting of the poloidal component

$$B_p(r) = \mu r^{-3}, \quad (6)$$

and μ is the NS magnetic dipole moment. Reconnection and opening of the field lines limit the magnitude of the toroidal com-

ponent to a fraction $\eta \lesssim 1$ of the poloidal component, and reduce the interaction layer to a width $(\Delta r/R_{\text{in}}) < 1$ (e.g. Wang 1996; Ghosh 2007; Lovelace et al. 1995; Romanova et al. 2009; D’Angelo & Spruit 2010). The magnetic torque integrated on such layer can be thus written as (see, e.g., D’Angelo & Spruit 2010):

$$\begin{aligned} T_m &= 2 \int [rS^{\text{m}}(r)] r dr d\phi = 4\pi S^{\text{m}}(R_{\text{in}}) R_{\text{in}}^2 \Delta r = \\ &= \pm \eta \left(\frac{\Delta r}{R_{\text{in}}} \right) \frac{\mu^2}{R_{\text{in}}^3}, \end{aligned} \quad (7)$$

where $[rS^{\text{m}}(r)]$ is the torque acting per unit area, and the factor 2 reflects the faces of the disc over which the torque is applied.

The sign of the magnetic torque exerted by the NS on the disc matter (Eq. 7) depends on the direction of the twist, and is positive when $\omega_* > 1$. In such conditions the neutron star deposits angular momentum into the disc, which makes feasible the ejection of matter along the field lines (i.e., a propeller state; Illarionov & Sunyaev 1975).

However, for values of ω_* between 1 and a certain critical value $\omega_*^{\text{cr}} \gtrsim 1$, the energy released by the propelling magnetosphere to the disc plasma is not sufficient to unbind it from the system (Spruit & Taam 1993). A large fraction of the propellered matter returns to the disc and builds up there, and may eventually resume accretion as it increases the inward accretion rate (see the recent works by D’Angelo & Spruit 2010, 2012, who examined in depth the cycles between accretion and angular momentum deposition at the inner rim, which takes place for values of $1 < \omega_* \leq \omega_{\text{cr}}$). For values of the fastness $\omega_* > \omega_*^{\text{cr}}$ the ejection of matter at the inner rim of the disc is instead clearly favoured, as the angular momentum and the energy which may be released by the NS to the disc matter increases. This tendency is also confirmed by the magneto-hydrodynamical simulations performed by Romanova et al. 2003; Ustyugova et al. 2006; Romanova et al. 2009. In the following, we consider a similar situation to model the phenomenology shown by XSS J12270–4859, and assume for simplicity that all the incoming matter is ejected by the system, $\dot{M}_{\text{ej}} = \dot{M}$.

Under the above assumptions, the conservation of angular momentum at the inner rim of the disc reads as:

$$\begin{aligned} \dot{M} R_{\text{in}} v_{\text{out}} &= (d/dt)L_{\dot{M}} + T_m = \\ &= \dot{M} \Omega_{\text{K}} R_{\text{in}}^2 + \eta \left(\frac{\Delta r}{R_{\text{in}}} \right) \frac{\mu^2}{R_{\text{in}}^3}, \end{aligned} \quad (8)$$

where, the term on the left hand side is the rate of angular momentum lost in the outflow, while the rate of angular momentum carried by disk matter (Eq. 4) and the torque applied by the magnetic field lines (Eq. 7) appear in the right hand side. Ekşi et al. (2005) proposed an useful parametrisation of the propeller process in terms of the elasticity of the scattering between the field lines and the disc plasma through a parameter β , which varies between $\beta = 1$ in the perfectly elastic case, and $\beta = 0$ in the purely an-elastic case. According to this parametrisation, the velocity of the outflow is:

$$v_{\text{out}} = \Omega_{\text{K}}(R_{\text{in}}) R_{\text{in}} [1 - (1 + \beta)(1 - \omega_*)]. \quad (9)$$

Substituting this relation in Eq.8 yields:

$$\omega_*^{7/3} (\omega_* - 1)(1 + \beta) = \frac{\eta (\Delta r/R_{\text{in}}) \mu^2}{\dot{M} \sqrt{GM} R_c^{7/2}}. \quad (10)$$

An ejecting propeller solution may hold only if the fastness exceeds the critical threshold, which was estimated by Perna et al. (2006) as:

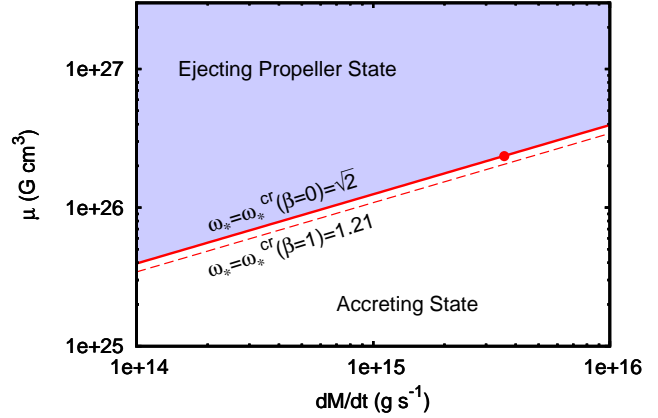


Figure 2. Values of the NS dipole moment and of the rate of mass lost by the disc giving the critical values of the fastness parameters, for a $1.4 M_{\odot}$ NS spinning a period of 2.5 ms, with $\eta = 1$ and $(\Delta r/R_{\text{in}}) = 0.1$. The red solid and dashed lines are evaluated for the critical fastness of the purely an-elastic and elastic case, respectively. These lines delimit the blue shaded region, where fully ejecting propeller solutions hold. The red circle marks the mass ejection rate evaluated for a system with a spin period of 2.5 ms, a luminosity of 10^{35} erg s^{-1} , and a fastness equal to the critical value.

$$\omega_*^{\text{cr}}(\beta) = \frac{\beta + \sqrt{2}}{1 + \beta}. \quad (11)$$

The critical threshold takes a value of 1.21 and $\sqrt{2}$ for the perfectly elastic ($\beta = 1$) and an-elastic ($\beta = 0$) case, respectively. We plot in Fig. 2 the values of the NS dipole moment and rate of mass lost leading to such critical values, which delimit the region where fully ejecting propeller solutions are possible.

The energy available to power the observed emission follows from the conservation of energy (Ekşi et al. 2005):

$$L_{\text{rad}} = \frac{GM\dot{M}}{R_{\text{in}}} + \Omega_* T_m - \frac{1}{2} \dot{M} v_{\text{out}}^2 = \quad (12)$$

$$= \frac{GM\dot{M}}{2R_{\text{in}}} [1 + (1 - \beta^2)(\omega_* - 1)^2], \quad (13)$$

and is related to the rate of mass in-flow (which equals the mass ejection rate under the assumptions made). Considering the critical fastness for the an-elastic case ($\omega_*^{\text{cr}} = \sqrt{2}$, $\beta = 0$), a spin period of 2.5 ms, and a value of the luminosity of 10^{35} erg s^{-1} (see Sec. 5.3), gives a mass ejection rate of 3.6×10^{15} g s^{-1} , which crosses the relative propeller solution for $\mu \gtrsim \text{few} \times 10^{26}$ G cm^3 (see the red circle in Fig. 2), of the order of the field usually estimated for NS in a LMXB.

In Sec. 5, we interpret the X-ray and *gamma*-ray emission of XSS J12270–4859 in terms of the synchrotron and self-synchrotron Compton emission by a population of relativistic electrons, accelerated by shocks at the magnetospheric interface of a propelling neutron star, and interacting with the NS magnetic field at the interface, \bar{B} . To estimate the strength of such field we consider a value of the order of the dipolar component of the NS field, evaluated at the inner disc radius:

$$\begin{aligned} \bar{B} &= B_p(R_{\text{in}}) = \frac{\mu}{R_{\text{in}}^3} = \frac{\mu}{R_c^3 \omega_*^2} = \frac{\mu \Omega_*^2}{GM_* \omega_*^2} = \frac{4\pi^2 \mu}{GM_* P^2 \omega_*^2} = \\ &= 0.85 \times 10^6 \mu_{26} P_{2.5}^{-2} (\omega_*/2)^{-2} G, \end{aligned} \quad (14)$$

where μ_{26} is the NS magnetic dipole moment in units of 10^{26} G cm^3 , and $P_{2.5}$ the spin period in units of 2.5 ms. The ex-

pression in the right hand side is obtained by using the definition of the NS fastness (Eq. 2), and the definition of the corotation radius (Eq. 3), considering a NS mass of $1.4 M_{\odot}$ (as implicitly assumed in the rest of the paper), taking a screening coefficient $\eta = 1$, and ignoring the tangential component introduced by shearing. The Eq. 14 implicitly expresses the NS magnetic dipole moment in terms of the field strength at the interface, the NS spin period, and the fastness, and can be plugged in the expression of the angular momentum conservation, Eq. 10. Further, \dot{M} can be expressed as a function of the radiated luminosity, spin period, fastness and elasticity parameter thanks to the relation expressing energy conservation, Eq. 12. Substituting in Eq. 10, and setting $\eta = 1$ and $(\Delta r/R_{\text{in}}) = 1$, finally yields:

$$\bar{B} = 5.2 \times 10^6 L_{35}^{-1} P_{2.5}^{-1/2} \left[\frac{1}{\omega_*} \frac{(\omega_* - 1) \times (1 + \beta)}{1 + (1 - \beta^2)(\omega_* - 1)^2} \right]^{1/2}. \quad (15)$$

Considering a spin period in a range typical of millisecond pulsars (1.5–5 ms), and a value of the fastness exceeding the critical threshold for mass ejection, ω_*^{cr} (Eq. 11), we conclude that the magnetic field at the interface \bar{B} must lie in a range between 2.2 and 11×10^6 G, to produce a total propeller luminosity of 1.5×10^{35} erg s $^{-1}$ (see Sec. 5.4 and Table 2).

It has to be noted that mass ejection is not a necessary outcome of a system in a propeller state. In fact, a steady solution for a thin disc with an angular momentum source at the inner rim exists for all values of $\omega_* > 1$ (Syunyaev & Shakura 1977). In such case, the angular momentum is retained in the disc, which readjusts by increasing its density with respect to the standard accreting solution, in order to match the increased demand of viscosity set by the source of angular momentum at the inner boundary. No mass in-flows in this case and the disc is considered *dead*. The angular momentum injected by the NS at the inner rim is released at the outer edge of the disc, most probably to the orbit of the binary through tidal interactions. Such state has been recently re-examined by D’Angelo & Spruit (2011, 2012). However, while a dead disc solution exists even if no matter is ejected by the system, it hardly holds on year-long time-scales such as those observed in XSS J12270–4859. As a matter of fact, if the disc is continuously replenished by a source of mass at a rate $\geq 10^{-12} M_{\odot} \text{ yr}^{-1}$, like those commonly observed from LMXB (e.g. Coriat et al. 2012), it takes the inward pressure of a *dead* disc only a few months to bring the inner disk radius back to the co-rotation surface. We then consider only the full-ejecting case discussed above as a possibility to explain the properties of XSS J12270–4859 in terms of a propeller state.

5 SPECTRAL ENERGY DISTRIBUTION

The plasma of the layer where the accretion disc is truncated in a propeller state is expected to be very turbulent and magnetised, as a result of the deposition of a copious amount of energy by the magnetosphere (see, e.g., magnetohydrodynamics numerical simulations studied by Romanova et al. 2009 and references therein). Such region was identified by Bednarek (2009b,a) as a suitable site to accelerate charged particles to relativistic energies through a Fermi process. Here, we apply a similar guess to the case of a relatively weakly magnetised ($B_{\text{NS}} \approx 10^{8-9}$ G, $\mu \approx 10^{26-27}$ G cm 3), quickly spinning ($P \approx$ few ms) NS in a LMXB, and study the spectral energy distribution expected to arise from the population of relativistic electrons expected to be produced at the layer between the magnetosphere and the disc. For simplicity, we

consider in the following that the electron distribution occupies a torus-like volume, with radial size equal to the inner disc radius $R_{\text{in}} = R_c \omega_*^{2/3}$ (see Eq. 2), and transverse section of size, R_t . Only the acceleration of electrons is considered in this model, while the possible contribution of hadrons is discussed in Sec. 5.5.

5.1 Electrons acceleration

In a Fermi acceleration process, energy is given up to each electron at a rate

$$\ell_{\text{acc}} = \xi c E / R_L = \xi e c B (R_{\text{in}}) = 1.4 \times 10^5 \xi_{0.01} \bar{B}_6 \text{ erg s}^{-1}, \quad (16)$$

where $R_L = E/eB$ is the Larmor radius, $\xi_{0.01}$ is the acceleration parameter in units of 0.01, e is the electron charge, and \bar{B}_6 is the strength of the magnetic field at the interface \bar{B} , in units of 10^6 G, which is of the order of the values determined in Sec. 4.

The time scale of electron acceleration is:

$$\tau_{\text{acc}} = \frac{\gamma m_e c^2}{\ell_{\text{acc}}} = 5.7 \times 10^{-8} \xi_{0.01} \bar{B}_6 (\gamma/10^4) \text{ s}, \quad (17)$$

where m_e is the electron mass. This value is much shorter than the time needed to travel the typical size of the region, R_{in} ,

$$\tau_{\text{tr}} = \frac{R_{\text{in}}}{c} = \frac{R_c \omega_*^{2/3}}{c} \approx 1.6 \times 10^{-4} P_{2.5}^{2/3} (\omega_*/2)^{2/3} \text{ s}, \quad (18)$$

ensuring that electrons can be effectively accelerated before that they can escape the system.

5.2 Emission processes and expected dominant components

The electrons accelerated by a Fermi process lose energy through the emission of radiation produced by their interaction with the magnetic and the radiation field permeating the transition layer, and with the ions of the plasma.

5.2.1 Synchrotron emission

Synchrotron losses proceed in the transition layer at the rate set by the Larmor formula:

$$\ell_{\text{syn}} = \frac{4}{9} \frac{e^4}{m_e^2 c^3} \bar{B}^2 \gamma^2 = 1.1 \times 10^5 \bar{B}_6^2 (\gamma/10^4)^2 \text{ erg s}^{-1}, \quad (19)$$

where γ is the electron Lorentz factor. If synchrotron losses are dominant over other channels of energy losses (see below), the parameters describing the electron energy distribution are set by the equilibrium between the energy injection through Fermi acceleration and synchrotron emission. In particular, the cut-off energy of the electron distribution is set by equating Eq. 16 and 19:

$$\gamma_{\text{max}}^{\text{syn}} = \frac{3}{2} \frac{m_e c^2}{e^{3/2}} \left(\frac{\xi}{\bar{B}} \right)^{1/2} = 1.2 \times 10^4 \xi_{0.01}^{1/2} \bar{B}_6^{-1/2}. \quad (20)$$

Assuming an exponentially cut power law distribution for the energy of the electrons:

$$\frac{dN_e}{d\gamma} = K \gamma^{-\alpha} \exp \left(-\frac{\gamma}{\gamma_{\text{max}}} \right), \quad (21)$$

the synchrotron spectral energy distribution is described by a power law:

$$(EF_E)^{\text{syn}} \propto E^{-(\alpha-3)/2} \exp \left[-\frac{3}{2} \left(\frac{E}{E_{\text{max}}^{\text{syn}}} \right)^{1/3} \right], \quad (22)$$

with cut-off energy:

$$E_{\max}^{\text{syn}} = \frac{3}{2} \frac{\hbar}{m_e c} \bar{B} (\gamma_{\max}^{\text{syn}})^2 = \frac{27}{16} \frac{\hbar m_e c^3}{e^2} \xi = 1.2 \xi_{0.01} \text{ MeV}. \quad (23)$$

(see, e.g., the relations given by Lefa et al. 2012, evaluated for an electron distribution like the one given by Eq. 21, and setting the electron Lorentz factor to the value given by Eq. 20). It results that when the synchrotron emission is the dominant cooling process, the cut-off energy of the emitted spectrum depends only on the acceleration parameter, ξ . This parameter may take values $\ll 1$ in the case of relativistic shocks, but it is largely undetermined on theoretical grounds (see Khangulyan et al. 2007, and references therein). In our model we assume that the main contribution to the 0.2–100 keV spectrum of XSS J12270–4859 (a power law $EF_E \propto E^{-(\Gamma_X - 2)}$, with an index $\Gamma_X = 1.70 \pm 0.02$ and no cut-off detected up to 100 keV, see Sec. 2 and 3) is given by synchrotron emission. Imposing that the cut-off energy of this component lies between 100 keV and 100 MeV, Eq. 23 can be used to constrain ξ to a broad range, 8.5×10^{-4} –0.85. Similarly the observed spectral slope indicates an electron energy distribution with $\alpha \simeq 2\Gamma - 1 = 2.4$. On the other hand, the high energy part of the spectrum observed by *Fermi*-LAT, with a cut-off at 4.1 ± 1.3 GeV (Hill et al. 2011), cannot be explained by synchrotron emission alone, as it would require $\xi \sim 30$, and is instead discussed in terms of (self-synchrotron) inverse Compton emission in Sec. 5.2.2.

At low energies the emitting region becomes optically thick to the synchrotron radiation. We evaluate the absorption coefficient for the relevant parameters of the system and an electron distribution with index $\alpha = 2.4$, following Rybicki & Lightman (1979):

$$\alpha_{\text{syn}}(E) = 3 \times 10^{-4} \left(\frac{n_e}{10^{17} \text{cm}^{-3}} \right) \bar{B}_6^{2.2} \left(\frac{E}{\text{eV}} \right)^{-3.2} \text{cm}^{-1}, \quad (24)$$

where n_e is the density of electrons of the considered medium, scaled to a value of the order of those obtained through modelling of the observed spectrum (see below). Imposing $\tau = \alpha_{\text{syn}}(E_{\text{br}}) R_t = 1$, we estimate the energy below which the medium becomes optically thick to synchrotron radiation as:

$$E_{\text{br}} = 2.9 \left(\frac{n_e}{10^{17} \text{cm}^{-3}} \right)^{0.31} \left(\frac{R_t}{\text{km}} \right)^{0.31} \bar{B}_6^{0.69} \text{eV}. \quad (25)$$

This value is between the optical and the UV band for typical parameters of the system, compatible with the absence of a low-energy cut-off in the observed X-ray data.

5.2.2 Inverse Compton emission

The weight of inverse Compton losses in the Thomson domain with respect to synchrotron losses can be evaluated as:

$$\frac{\ell_{\text{IC}}}{\ell_{\text{syn}}} = \frac{\epsilon_{\text{ph}}}{\epsilon_{\text{mag}}}, \quad (26)$$

where ϵ_{ph} and $\epsilon_{\text{mag}} = \bar{B}^2/8\pi$ are the energy density in the radiation and in the magnetic field, respectively.

The inner rings of a viscous disc emit thermal photons with typical temperature set by amount of angular momentum that has to be dissipated by the disc. This is related to the rate of mass inflow (here set equal to the rate of mass lost) and by the size of the disc (Frank et al. 2002), yielding $kT(R_{\text{in}}) \approx 100$ eV for $\dot{m}_{1.5} = P_{2.5} = 1$ and $\omega_* = 2$. Even ignoring the reduction of the cross section for inverse Compton scattering of photons with initial energy lower than the Klein-Nishina threshold $\approx m_e c^2/4\gamma$ (≈ 10 eV for $\gamma = 10^4$), the energy density implied by a similar thermal spectrum, $\epsilon_{\text{disc}} = aT^4(R_{\text{in}})$, is lower by more than a factor

1000 than the density associated to a 10^6 G magnetic field. Inverse Compton scattering of disc photons is then energetically unimportant with respect to synchrotron emission, for typical parameters of the systems considered here,

Photons emitted by the low mass companion have an even lower density at the interface between the disc and the magnetosphere, $\epsilon_{\text{star}}/\epsilon_{\text{disc}} \approx [T_2/T(R_{\text{in}})]^4 (R_2/a)^2 \approx 10^{-10}$, where T_2 and R_2 are the companion star temperature and radius, respectively, and a is the size of the orbit. To evaluate such ratio we considered $T_2 \simeq 4600$ K, $R_2 \approx 0.6R_\odot$, a total mass of the system of $2M_\odot$, and an orbital period of 8 hr, values typical of a late type K star as proposed by De Martino et al. (2013).

On the other hand, inverse Compton scattering of the synchrotron photons off the same electron population which produced them (synchrotron self Compton process; SSC in the following) may play an important role if the electron distribution is concentrated in a relatively small region, such as the transition region that we are considering here ($R_{\text{in}} \approx 50$ km, $R_t \approx$ few km). In the Thomson regime, the ratio between the luminosity emitted through synchrotron and SSC process is (e.g. Sari & Esin 2001):

$$\frac{L_{\text{SSC}}}{L_{\text{syn}}} \sim \frac{1}{3} \frac{E_{\max}^{\text{SSC}}}{E_{\max}^{\text{syn}}} \sigma_T n_e R_{\text{in}}, \quad (27)$$

where E_{\max}^{SSC} and E_{\max}^{syn} are the peak energies of the SSC and synchrotron photons. While the latter energy is set by Eq. 23, the cut-off of the inverse Compton distribution reproduces that of the electron energy distribution, $E_{\text{SSC}}^{\text{max}} = \gamma_{\max} m_e c^2$. Taking into account also the SSC losses, and defining $f \equiv 1 + L_{\text{SSC}}/L_{\text{syn}}$, the maximum energy that can be achieved by the electron distribution is then obtained by balancing electron energy losses and gains,

$$\ell_{\text{syn}} + \ell_{\text{SSC}} = f \ell_{\text{syn}} = \ell_{\text{acc}}, \quad (28)$$

yielding:

$$\gamma_{\max}^{\text{SSC}} = \frac{\gamma_{\max}^{\text{syn}}}{\sqrt{f}} = 8.2 \times 10^3 f_2^{-1/2} \xi_{0.01}^{1/2} \bar{B}_6^{-1/2}. \quad (29)$$

Here, we defined $f_2 = f/2$, to scale the energy ratio to the case of an equal luminosity released by synchrotron and SSC processes. The SSC spectrum is then cut-off at an energy of:

$$E_{\text{SSC}}^{\text{max}} = 4.2 f_2^{-1/2} \xi_{0.01}^{1/2} \bar{B}_6^{-1/2} \text{GeV}. \quad (30)$$

of the order of that observed from XSS J12270–4859 by *Fermi*-LAT (4.1 ± 1.3 GeV; Hill et al. 2011). SSC emission can be thus responsible of the γ -ray flux observed from XSS J12270–4859 and perhaps from other binaries. By setting the high-energy cut-off of the spectrum to the observed value, and varying the magnetic field in the range determined in Sec. 4 ($\bar{B}_6=2.2$ –11), Eq. 30 shows that the ratio of the luminosity emitted by SSC and synchrotron process depends linearly on the poorly constrained acceleration parameter, ξ . If the latter is varied in the range determined in Sec. 5.2.1 by imposing that the cut-off of the synchrotron spectrum lies between 100 keV and 100 MeV ($\xi = 8.5 \times 10^{-4}$ –0.85), values of f ranging from $\sim 10^{-2}$ to 40 are obtained. It is then clear that a sensible estimate of the expected flux ratio cannot be given without an accurate knowledge of the acceleration parameter. On the other hand, as XSS J12270–4859 emits a comparable γ -ray and X-ray flux, we expect the two components to emit energy at a comparable rate. By setting $f = 2$ in Eq. 30, we can therefore constrain the acceleration parameter to lie in the range $\xi = 0.02$ –0.10, in order to reproduce the observational features of XSS J12270–4859, in the framework set by our model.

At zero order, the electron density requested to produce a similar contribution from SSC and synchrotron emission ($L_{\text{SSC}}/L_{\text{syn}} = 1$, $f = 2$) can be estimated from Eq. 27:

$$n_e \approx 2.7 \times 10^{14} f_2^{-1/2} \xi_{0.01} P_{2.5}^{-2/3} (\omega_*/2)^{-2/3} \text{ cm}^{-3}. \quad (31)$$

However, this value is largely underestimated as the reduction of the cross section due to Klein Nishina effects largely decreases the efficiency of the SSC emission. We show in Sec. 5.3 how densities of the order of 10^{17} cm^{-3} are needed to reproduce the observed spectral energy distribution.

This value of the electron density has to be compared with the expected density in the outflow. By imposing mass continuity at the base of the outflow, we estimate a scale unit of the mass density as:

$$\begin{aligned} \rho_0 &= \frac{\dot{M}}{2\pi R_{\text{in}} R_t v_{\text{out}}} = \\ &= 10^{-7} \dot{m}_{15} P_{2.5}^{-1/3} (\omega_*/2)^{-4/3} (R_t/10^5 \text{ cm}) \text{ g cm}^{-3}, \end{aligned} \quad (32)$$

where we used Eq. 9 to express the outflow velocity in the purely ejecting case ($\beta = 1$), and considered a typical size for the transverse section of the acceleration region $R_t \approx 10^5 \text{ cm}$ (see below). For a fully ionised plasma, the electron density is therefore:

$$n_{e,0} \simeq \frac{\rho_0}{m_H} (X + Y/2) \approx 0.5 \times 10^{17} \text{ cm}^{-3}, \quad (33)$$

where we omitted the dependencies on the scale units used so far, and we considered solar abundances for hydrogen and helium, $X = 0.7$ and $Y = 0.28$, respectively. Such a value of the scale unit of electron density is not far from that needed to produce a comparable SSC and synchrotron emission ($\approx \text{few} \times 10^{17} \text{ cm}^{-3}$; see Sec. 5.3).

5.2.3 Bremsstrahlung emission

To evaluate the energy lost by electrons in bremsstrahlung interactions with the ions of plasma, we considered the relation given by Blumenthal & Gould (1970), in the approximation of a fully ionised plasma:

$$\begin{aligned} \ell_{\text{brems}} &= \frac{4e^6}{\hbar m_e^2 c^4} (2n_H + 20n_{He}) [\log(2\gamma) - 1/3] \gamma m_e c^2 \simeq \\ &0.66 \left(\frac{\rho}{\rho_0} \right) \left(\frac{\gamma}{10^4} \right) \text{ erg s}^{-1}. \end{aligned} \quad (34)$$

Here $n_H = X\rho/m_H$ and $n_{He} = Y\rho/m_H$ are the hydrogen and helium number densities, respectively, and a solar composition is considered. By comparing this relation to energy gains and other radiative losses (see Eq. 16, 19 and 28), we deduce that bremsstrahlung radiation is not dominant for the typical densities of a propeller outflow.

5.2.4 Coulomb losses

Energy losses through Coulomb interactions can be safely ignored for the relevant parameters. Considering the rate of energy lost by a relativistic population of electrons through Coulomb interactions with other electrons and with much less energetic ions (e.g. Frankel et al. 1979), a slowing down time scale:

$$\tau_{\text{coll}} \simeq 130 (\gamma/10^4) (\rho/\rho_0)^{-1} \text{ s} \quad (35)$$

is obtained, much longer than other time scales of the system.

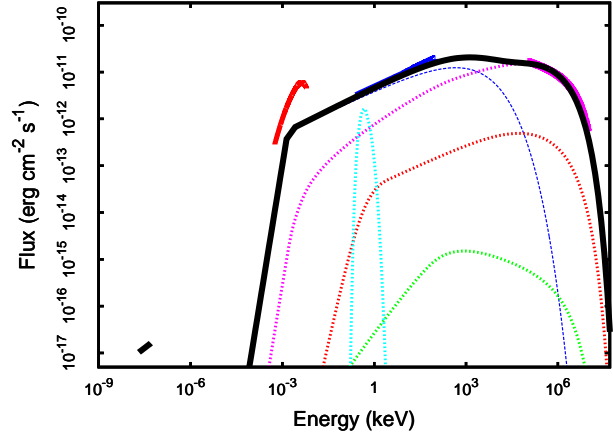


Figure 3. Spectral energy distribution observed from XSS J12270–4859 in the γ -rays, X-rays, IR/optical/UV and radio bands (magenta, blue, optical and black thick lines, respectively). The model obtained for $\alpha = 2.4$, $\gamma_{\text{max}} = 10^4$, $\bar{B} = 5 \times 10^6 \text{ G}$ and $n_e = 12 \times 10^{17} \text{ cm}^{-3}$ is over-plotted as a black line. The components due to the synchrotron, SSC, inverse Compton of disc photons, and bremsstrahlung in the relativistic plasma are shown as blue, magenta, red and green dotted lines, respectively. The cyan dashed line represents the possible contribution of the inner parts of an accretion disk truncated at a radius of 50 km, with an inner temperature of 0.1 keV, an inclination of 75° , and absorbed by the interstellar medium with an absorption column $N_{\text{H}} = 10^{21} \text{ cm}^{-2}$ (De Martino et al. 2010). This component has not been taken into account in evaluating the model, considering the large uncertainties on the actual emission of a disk in a propeller state.

5.3 Simulated spectral energy distribution

To estimate quantitatively if the proposed model can reproduce the broad-band spectral energy distribution observed from XSS J12270–4859, we modelled the radiation processes described in the previous section (synchrotron, SSC, inverse Compton scattering of the disc photons, and bremsstrahlung) using the codes described by Torres (2004), de Cea del Pozo et al. (2009) and Martín et al. (2012), and assuming a distance to the system of 2 kpc.

The electron distribution for $\gamma > 1$ is described by an exponentially cut-off power law (Eq. 21). The energy distribution and luminosity produced by the synchrotron and SSC processes also depend on the strength of the magnetic field interacting with the electrons, \bar{B} , and on the electron density, n_e respectively.

We set the model parameters to reproduce the $\Gamma_1 = 1.70 \pm 0.02$ power law observed in the 0.2–100 keV band by *XMM-Newton*, *RXTE* and *INTEGRAL* (with an unabsorbed flux of $(4.5 \pm 0.9) \times 10^{-11} \text{ erg cm}^{-2} \text{ s}^{-1}$; De Martino et al. 2010, 2013), and the $\Gamma_2 = 2.21 \pm 0.09$ power law, cut off at $E_{\text{cut}} = 4.1 \pm 1.3 \text{ GeV}$, observed above 100 MeV by *Fermi-LAT* (with an unabsorbed flux of $(4.1 \pm 0.3) \times 10^{-11} \text{ erg cm}^{-2} \text{ s}^{-1}$, Hill et al. 2011). The spectral energy distribution of these two components is plotted as a blue and magenta thick line in Fig. 3, respectively, together with the IR/optical/UV (red thick line; De Martino et al. 2013) and the radio spectrum (black thick line; Hill et al. 2011).

The cut-off in the γ -ray energy band is well reproduced by $\gamma_{\text{max}} = 10^4$. On the other hand, the shape of the X-ray power law results from the sum of the synchrotron and SSC contribution in that energy band (with the former contributing for more than two thirds of the emission), and is reasonably modelled by using an index $\alpha = 2.4$ for the electron energy distribution. Keeping fixed these two parameters, and choosing $\bar{B} = 5 \times 10^6 \text{ G}$, we found

Table 2. Model parameters reproducing the X-ray to γ -ray spectrum observed from XSS J12270–4859. The cut-off of the electron distribution is fixed at $\gamma = 10^4$ and $\alpha = 2.4$. A distance of 2 kpc is considered.

\bar{B} (MG)	$n_{e,17}$ (cm $^{-3}$)	$L_{\text{syn};35}$	$L_{\text{SSC};35}$	ξ	ω_*	β	μ_{26} (G cm 3)	\dot{m}_{15} (g s $^{-1}$)	R_{in} (km)	R_t (km)
1	2.6	0.48	0.77	0.019	1.03	...	0.3	...	31	1.3
3	4.9	0.62	0.67	0.046	1.40–1.44	0 – 0.1	1.7 – 1.8	4.5 – 4.6	38 – 39	0.3 – 0.4
4	7.0	0.73	0.71	0.059	1.3 – 1.70	0.40 – 1	1.9 – 3.4	4.8 – 5.6	36 – 44	0.20 – 0.22
5	12	0.77	0.72	0.072	1.4 – 1.9	0.76 – 1	3.1 – 5.4	5.6 – 6.2	39 – 48	0.12 – 0.13
6	12	0.78	0.69	0.083	1.8 – 2.4	0.93 – 1	5.8 – 10	7.0 – 7.3	46 – 56	0.09 – 0.10

a good modelling of the observed X-ray and γ -ray spectra for an electron density of $n_e = 12 \times 10^{17}$ cm $^{-3}$. The spectral energy distribution so obtained is plotted in Fig. 3 as a black solid line, where the synchrotron and SSC components are also drawn as a blue and magenta dotted line, respectively. The low energy cut-off of the synchrotron spectrum is set at the energy predicted by Eq. 25.

In Fig. 3, we also plot the inverse Compton spectrum yielded by seed photons coming from the inner disk (assuming an inner temperature of 100 eV and a truncation radius of 50 km) and the bremsstrahlung spectrum (evaluated for a fully ionised plasma with an electron density equal to the value determined above) as a red and green dotted line, respectively. Their contribution to the total spectrum can be then safely neglected, for the parameters considered in this case, according to expectations.

Similarly, the thermal X-ray output of the inner parts of the truncated accretion disk is expected to be at most of the same order of the synchrotron emission, at energies of few tenths of keV. To show this, we used the model developed by Gierliński et al. (1999) to model the spectrum of an disk in the accreting high state, truncated at 50 km, with an inner disk temperature of 100 eV (see Sec. 5.2.2), a high inclination of 75° (as possibly indicated by the dips and flares observed from the source), a hardening factor of 2, and interstellar absorption by a column with density $N_{\text{H}} = 10^{21}$ cm $^{-2}$ (see cyan dashed line in Fig. 3). This component would have a 0.5–10 keV flux not larger than a factor of few with respect to the upper limit which can be set on the presence of a disk thermal component during the January 2009 observation (2×10^{-13} erg cm $^{-2}$ s $^{-1}$). Considering the large uncertainties on the thermal emission of an disc truncated by a propeller magnetosphere, and the scattering of most of the disk soft X-ray photons by the electron cloud (see red dashed line in Fig. 3), we then consider that the non detection of a thermal component at soft X-rays is still compatible with our description.

The IR/optical/UV spectrum was modelled by De Martino et al. 2013 as the sum of the contributions of the companion star ($T_2 = 4600 \pm 250$ K) and of the outer part of the accretion disc ($T_h = 12800 \pm 600$ K; $R \approx 10^5$ km). Considering also the low energy cut-off of the synchrotron spectrum at few eV, the emission coming from the transition layer is not expected to contribute directly to more than ten per cent to the IR/optical/UV output. However, UV flares are simultaneous to X-ray flares, despite they have a lower amplitude, by a factor of two, indicating that the emission in the two bands are closely related (De Martino et al. 2010, 2013). This is still compatible with our model if the UV emission is assumed to be due to reprocessing in the outer rings of the disc of the X-ray emission generated at the inner disc boundary, something already suggested by De Martino et al. 2013.

The emission model that we have developed for the radiation coming from the transition layer cannot explain the optically

thin/flat radio spectrum ($F_E \sim \nu^p$, with $p = -0.5 \pm 0.6$) observed by ATCA at frequencies of 5.5 and 9 GHz (Hill et al. 2011). It is evident from Eq. 25 that a similar emission has to come from a region of a larger size, with a correspondingly lower electron density and magnetic field strength. For instance, in order to obtain a break of the synchrotron spectrum below 5.5 GHz, and assuming a dipolar decay of the field as $B(r) \propto r^{-3}$, the emitting region should be 100 times larger and have a density lower by four orders of magnitude. These properties would be anyway compatible with an emitting region pertaining to the binary system.

5.4 Implications for XSS J12270–4859

The model parameters that we obtained can be used together with the relation derived in Sec. 4 and 5, to get model-dependent constraints on the system parameters. The cut-off energy of the electron distribution ($\gamma = 10^4$) and the magnetic field strength at the interface ($\bar{B} = 5 \times 10^6$ G), are related by Eq. 29 to the acceleration parameter ξ , and the ratio between the synchrotron and the SSC luminosity, f . For the considered parameters, we have $f = 1.98$ and an acceleration parameter $\xi \simeq 0.07$ (see Table 2).

Eq. 15 relates the strength of the field at the interface to the radiated luminosity, the spin period, the fastness and the elasticity parameter. Setting $P_{2.5} = 1$, and the luminosity of 1.49×10^{35} erg s $^{-1}$ as obtained from our modelling, gives a fastness parameter of 1.45 for the elastic propeller case (larger than the critical value of 1.21 needed for mass ejection, Perna et al. 2006), a magnetic dipole moment of 3.1×10^{26} G cm 3 (Eq. 14) and a mass ejection rate of 6.3×10^{15} g s $^{-1}$ (Eq. 8), compatible with the typical mass accretion rates observed from NS in LMXB. For these parameters, the inner disc radius would be placed at $R_{\text{in}} \simeq 40$ km, with an acceleration region of transverse section $R_t \simeq 0.1$ km.

We also varied the strength of the magnetic field at the interface \bar{B} to study the range of parameters which lead to a good fit of the observed spectral energy distribution, and compatible with the propeller model developed in Sec.4. Decreasing \bar{B} while keeping fixed the spin period, increases the range of values of the elasticity parameters which can provide a solution above the value of the critical fastness. For instance, a value of $\bar{B}_6 = 4$ gives a propeller solution for $\beta > 0.4$, while $\bar{B}_6 = 3$ is allowed for $0.1 > \beta > 0$. A similar effect is obtained by increasing the value of the spin period. A too low value of the field (e.g. $\bar{B}_6 = 1$) at the interface is not formally compatible with the propeller model we developed; in this case, in fact, a solution of Eq. 15 is found for $\omega < 1.03$, which is below the critical fastness for any elasticity parameter. For such values the field would then more likely produce an accretion state than a propeller. On the other hand, when \bar{B} is increased above 6×10^6 G, the volume of the acceleration zone needed to keep the contribution of the SSC photons comparable to that yielded by synchrotron photons, decreases uncomfortably, while the acceleration

parameter goes above a value of 0.1. At the same time the magnetic dipole moment increases above 10^{27} G cm³, which is also unlikely for a NS in a LMXB. We therefore conclude that an interface magnetic field strength in a relatively narrow range of $3\text{--}6 \times 10^6$ G best reproduces the observed spectra and is compatible with the theoretical expectations for a NS in a LMXB, ejecting mass in a propeller state. This range of field imply an acceleration parameter in the range 0.04–0.08, to give a comparable emission in the two components (see Eq. 29). The parameter values of a sample set of models are given in Table 2.

5.5 Hadrons acceleration

So far, we have not analysed possible acceleration of hadrons, followed by subsequent interactions with material in the disc, pion decay, and gamma-ray production. This is an alternative that may in principle require consideration. In our scenario, where particles get accelerated in the transition zone, use of Eq. 17 and 18, which give the timescale of acceleration and escape, applied to the case of protons, imply that the maximum proton acceleration would happen for a Lorentz factor of 10^4 , i.e., an energy of 10 TeV. We do not see the outcome of these accelerated protons, which would produce photons up to a few hundreds GeV, since the gamma-ray spectrum is severely cut at a few GeV. (For electrons, the maximum energy of the population is limited not by escape losses, but by synchrotron and SSC, which can be instead neglected in the case of protons, as they are a factor $(m_p/m_e)^2 \approx 4 \times 10^6$ less efficient, see Eq. 19) One could in principle entertain that protons of the highest energies will penetrate the inner structure of the accretion disc, and interacting there would produce a photon of few 100 GeV which would very likely interact as well, being absorbed (see, e.g., Bednarek 1993). We cannot discard this scenario a priori, without detailed computations, as a possible contributor to the total SED yield. What may seem less likely is the picture in which the protons are accelerated in an electrostatic gap out of the transition zone, which then impact the accretion disk in a sort of beam-meets-target phenomenon (Cheng & Ruderman 1989). This scenario has been explored for some high-mass X-ray binaries, like A0535+26 (earlier claimed as a possible EGRET source) by Romero et al. (2001), and Anchordoqui et al. (2003); albeit the model has not been confirmed by Fermi-LAT or at higher energies (Acciari et al. 2011). In our case, assuming first we are in accretion phase, not in propeller, and using the formulae in Romero et al. 2001, the acceleration potential would produce one order of magnitude less voltage than for A0535+26, and the current flowing in the disc would also be one order of magnitude less.

6 DISCUSSION

Being the only LMXB with a proposed bright persistent γ -ray counterpart discovered so far, XSS J12270–4859 is an extremely intriguing source. Though, the nature of the compact object hosted by this system is still uncertain. In this paper, we proposed that the system hosts a neutron star in a propeller state, developing a model to reproduce the observed X-ray and γ -ray properties of the source. Before discussing the implication of the model we presented in this paper, we briefly summarise other possibilities suggested to explain at least partly the rich phenomenology observed from XSS J12270–4859.

6.1 Can it be a rotational-powered pulsar?

Coherent pulsations were not detected from XSS J12270–4859 in the X-ray and radio band, nor from its proposed γ -ray counterpart. The upper limit on the X-ray pulse amplitude set by (De Martino et al. 2013, between 15 and 25 per cent in the 0.5–10 keV band) are larger than those observed from many accreting millisecond pulsars (see, e.g. Patruno & Watts 2012, and references therein), and should not be considered particularly constraining as to whether an accreting pulsar is present in the system.

On the other hand, the non detection of radio pulsations reported by Hill et al. (2011) on the basis of Parkes 1.4 GHz observations indicates that if XSS J12270–4859 harbours a rotation powered pulsar, either its pulsed emission is not beamed towards the Earth, or it is scattered and absorbed by matter engulfing the system. Indeed, the similarity of the γ -ray spectrum of the proposed counterpart of XSS J12270–4859 to those observed by Fermi from several γ -ray pulsars, led Hill et al. (2011) to suggest that the system may host a similar radio quiet/faint γ -ray pulsar. However, we note that the X-ray emission of XSS J12270–4859 ($L_X = 6.5(1) \times 10^{33}$ erg s^{−1} in the 2–10 keV band) is larger by orders of magnitude than that expected and usually observed from rotation powered pulsars with a low mass companion. In fact, similar systems usually harbour a weakly magnetised ($B \simeq 10^8\text{--}10^9$ G) pulsar, spun up to a millisecond spin period by a previous phase of mass accretion (see, e.g. Bhattacharya & van den Heuvel 1991). Expressing the spin-down power of a pulsar as

$$\dot{E} \approx \frac{\mu^2}{c^3} \left(\frac{2\pi}{P} \right)^4, \quad (36)$$

with μ magnetic dipole moment, and P the spin period of the neutron star, and considering a $\eta = L_X/\dot{E} \leq 10^{-3}$ efficiency of the conversion of the spin down power in X-ray luminosity (e.g. Becker 2009), typical parameters observed in millisecond pulsars ($P \approx$ few ms; $\mu \approx 10^{26}$ G cm^{−3}) yield:

$$L_X^{\dot{p}sr} \simeq 1.5 \times 10^{31} \eta_{-3} \mu_{26}^2 P_{2.5}^{-1} \text{ erg s}^{-1}. \quad (37)$$

Here, η_{-3} is the X-ray conversion efficiency in units of 10^{-3} . Indeed, the brightest rotation powered millisecond pulsars in X-rays have luminosities of $\simeq 10^{33}$ erg s^{−1} (Cusumano et al. 2003; Webb et al. 2004; Bogdanov et al. 2011). Similarly, pulsars which showed a transition between rotation and accretion powered states, PSR J1023+0038 (Archibald et al. 2009), and IGR J18245–2452 (Papitto et al. 2013), were observed at an X-ray luminosity of $\approx 10^{32}$ erg s^{−1} during their rotation powered activity (Archibald et al. 2010; Bogdanov et al. 2011). To match a similar value, XSS J12270–4859 should be then closer than 0.6 kpc, spinning rather rapidly and/or being particularly young. We note that a distance 1.4–3.6 kpc is suggested by the spectral shape of the colder thermal component detected in the optical band by De Martino et al. (2013).

Also, the observation of optical emission lines would not seem to easily fit a scenario with a rotation powered pulsar, as in a similar state the pulsar wind would be expected to sweep the entire Roche Lobe of the neutron star from the matter transferred by the companion star (Ruderman et al. 1989). For similar reasons we consider the rotation powered pulsar scenario is at least improbable, as XSS J12270–4859 should be by far the brightest rotation powered pulsar, without pulsations being detected, and with a disk surviving the intense radiation pressure which would be implied by such a high spin down power.

6.2 Can it be an accreting black hole?

The non-detection of coherent pulsations from XSS J12270–4859 and its short term X-ray variability leaves open the possibility that an accreting black hole in a low hard state is present in the system (Saitou et al. 2009; De Martino et al. 2013). In such case, the radio emission would be originated in a compact jet. Indeed, the largely uncertainty of the radio spectrum (a $F_\nu \propto \nu^{-\alpha}$ power-law spectrum, with $\alpha = 0.5 \pm 0.6$) makes it compatible with the typical flat spectrum observed from compact jets ($\alpha \approx 0$). As noted by De Martino et al. (2013), the observed ratio between the radio luminosity at 9 GHz and the X-ray luminosity in the 3–9 keV X-ray band place it slightly under-luminous in the radio band with respect to the correlation observed for black hole binaries (Gallo et al. 2003), while it seems over-luminous with respect to accreting neutron stars in the hard state (Migliari & Fender 2006). However, the relatively bright gamma-ray emission seems difficult to reconcile with a black-hole scenario. So far, GeV emission has been detected only from two systems hosting a black hole; a weak emission recently detected from Cyg X-1 (Malyshev et al. 2013) –albeit this has not been confirmed in subsequent analysis by the *Fermi*-LAT collaboration–, and a brighter but transient emission observed from Cyg X-3 (Tavani et al. 2009; Fermi LAT Collaboration et al. 2009). In both cases, however, according to leptonic models the high energy emission is related to up-scattering of the dense photon field emitted by the massive companion star and/or the disc, which are hardly important contributors in the case of XSS J12270–4859. Indeed, no gamma-ray emission has been reported so far from the many black holes with a low-mass companion star known. Thus we also consider this scenario unlikely.

6.3 A neutron star in propeller

In this paper we have proposed a propeller neutron star scenario for XSS J12270–4859. Our model is based on the assumption that in a similar state a population of electrons can be accelerated to relativistic energies at the interface between the disc and the magnetosphere, following the suggestion put forward by Bednarek (2009b,a). He applied a similar model to the case of slowly rotating ($P \gtrsim 10$ s) accreting NS in HMXB ($B_{\text{NS}} \sim 10^{12}$ G, $\mu \sim 10^{30}$ G cm³; Bednarek 2009a), as well as to NSs with super-critical magnetic field at their surface ($B_{\text{NS}} \sim 10^{14}$ G, $\mu \sim 10^{32}$ G cm³), harboured in binary system with a massive companion star (Bednarek 2009b). This concept was later developed by Torres et al. (2012); Papitto et al. (2012) to explain the multi-wavelength phenomenology of LS I 61 303; and has found support in the recent discovery of the super orbital variability of the gamma-ray emission from the system (Ackermann et al. 2013).

While the surface magnetic field of a typical NS in a LMXB is lower by more than four orders of magnitude than the much more intense fields of NS in HMXB or in magnetars, the radius at which the matter in-flow is truncated in a NS-LMXB system is much lower. The field at the magnetospheric interface of a NS in a LMXB, like that hypothesised for XSS J12270–4859, is then up to three orders of magnitude larger in this case (Eq. 14), and as a consequence also the power available to accelerate electrons (Eq. 16).

For typical parameters of a system like the one considered here, the cooling of this electron population takes place mainly through synchrotron interaction with the magnetic field permeating the interface, and through inverse Compton losses due to the interaction between the electrons and the synchrotron photons. The dominance of self-synchrotron Compton emission is not usually

encountered in systems. We found that LMXB in a propeller state could be prone to this situation. Inverse Compton losses given by the interaction with the radiation field emitted by the disc, and by the companion star, represent in fact a contribution which is orders of magnitude lower. The same holds for bremsstrahlung losses.

As both the dominant cooling channels are strongly dependent on the strength of the magnetic field, this quantity has a crucial influence on the value of the maximum energy yielded to electrons. We showed that for typical parameters of a propeller NS in LMXB ($\mu \approx \text{few} \times 10^{26}$ G cm³, $P \approx \text{few ms}$, $R_{\text{in}} \gtrsim 50$ km), and an acceleration parameter in the range 0.01–0.1, a maximum energy of few GeV is naturally obtained, compatible with the high energy cutoff observed from the γ -ray counterpart of XSS J12270–4859. At the same time, if the emission region is compatible with the size of the magnetosphere-disc interface ($R_{\text{in}} \gtrsim 50$ km; $R_t \approx \text{km}$), the synchrotron self Compton emission will give rise to an emission with an overall output comparable to that yielded in X-rays by the synchrotron emission. A similar model is therefore able to explain semi-quantitatively the peculiar spectral energy distribution of XSS J12270–4859 at high energies. On the other hand, synchrotron absorption in the emission region predicts a low energy cut-off at few eV. According to our model, the emission arising at the magnetospheric interface cannot take into account the radio emission observed from the source, which should therefore come from a larger region with a lower electron density.

The model we presented may also explain the observational features recently observed from the transitional pulsar PSR J1023+0038. Following the disappearance of radio pulsations, the onset of an accretion state has been recently reported for this otherwise rotational-powered system (Stappers et al. 2013). Evidences supporting the formation of an accretion disc has been obtained from optical observations (Halpern et al. 2013), similar to those which let Archibald et al. (2009) to conclude that the source was in an accretion state between 2000 and 2001 (see also Wang et al. 2009). Simultaneously, the source brightened by more than an order of magnitude in X-rays to an average level of $L_X(0.5\text{--}10 \text{ keV}) \simeq 2.5 \times 10^{33}$ erg s^{−1} (with variations by a factor 10 on timescales of few tens of seconds Patruno et al. 2013; Kong 2013; Papitto et al. 2013), and by at least a factor of five in gamma-rays ($L_\gamma(> 100 \text{ MeV}) \gtrsim 5 \times 10^{33}$ erg s^{−1}, Stappers et al. 2013), with respect to the rotation-powered phase characterised by an active radio-pulsar (Archibald et al. 2010; Tam et al. 2010; Bogdanov et al. 2011). The observed value of the X-ray luminosity strongly suggests that the system has entered a propeller state, possibly alternating with a rotational-powered state on short timescales of tens of seconds (Patruno et al. 2013). The model we presented can be taken as a plausible interpretation of the comparable emission observed from this system in X-rays and gamma-rays, alternative to a scenario in which the gamma-ray emission is due exclusively to residual periods of activity as a rotational-powered pulsar.

In the model presented here we considered a neutron star in a purely ejecting propeller state, even if Bednarek (2009b,a) argued that the electron acceleration at the magnetospheric interface can take place both if the neutron star is effectively accreting the in-flowing mass down to its surface, and if it is instead propeller-ing mass away. Such a choice was made as in such conditions the interface between the field and the disc is expected to be highly turbulent and magnetised, thus favouring the acceleration of electrons through a Fermi process. Even if the accretion of a fraction of the in-flowing matter (like in the trapped state studied by D’Angelo & Spruit 2010, 2012 and applied by Patruno et al. 2009; Patruno & D’Angelo 2013 to interpret properties of a few accreting

pulsars) is in principle possible, the low X-ray flux observed from the source and the absence of a detected thermal component in the soft X-ray band set a limit on the accretion rate. Even assuming that the total X-ray output of the source is powered by accretion, this would not take place at a rate larger than $\simeq 2 \times 10^{-12} M_{\odot} \text{ yr}^{-1}$, i.e. 10^{-4} times the Eddington rate.

According to our model, the observed X-ray and gamma-ray emission (as well as the matter outflow) are ultimately powered by the in-fall of matter down to the disc truncation radius, and by the energy deposited by the rotating magnetosphere (see Eq. 12). The observed X-ray flares/dip pairs could be then produced by a sudden increase of the rate of mass in-fall, caused by inhomogeneities of the disc accretion flow, and a subsequent re-fill of the starved parts of the disc, similar to the interpretation given by De Martino et al. 2010, 2013. On the other hand, the observed UV emission is larger by an order of magnitude than the contribution of the synchrotron component of our model at those energies. To explain the simultaneity among flares and dips observed at X-rays and UV energies, we should then conclude that the latter emission is mainly due to reprocessing in the outer parts of the disc, of the emission at higher energies produced close to the magnetospheric boundary.

As a concluding remark, we note that positional correspondences between persistent and transient X-ray binaries and γ -ray sources detected by Fermi and Agile seem intrinsically rare (e.g. Ubertini et al. 2009; Sguera et al. 2011; Li et al. 2012, and references therein). Maselli et al. (2011) searched for positional correspondence between sources of the second Palermo BAT catalogue (Cusumano et al. 2010) and the first Fermi catalogue (Abdo et al. 2010) and found only 15 galactic sources, among which only two are LMXB, XSS J12270–4859 and SLX 1735–269. Intriguingly, also the latter is a faint persistent X-ray source, and on this basis was classified by in’t Zand et al. (2007) as a candidate ultra-compact X-ray binary. The increase in sensitivity obtained by Fermi as its mission progresses will help shedding light on the possibility that more γ -ray LMXB candidates exist; at least, in those cases where the accretion state is such that a steady gamma-ray emission exist.

ACKNOWLEDGMENTS

Work done in the framework of the grants AYA2012-39303, as well as SGR2009-811, and iLINK2011-0303. AP is supported by a Juan de la Cierva Research Fellowship. DFT was additionally supported by a Friedrich Wilhelm Bessel Award of the Alexander von Humboldt Foundation. AP thanks D. De Martino for illuminating discussions.

REFERENCES

Abdo A. A., et al., 2010, *ApJS*, 188, 405
 Acciari V. A., et al., 2011, *ApJ*, 733, 96
 Ackermann M., et al., 2013, *ApJ*, 773, L35
 Anchordoqui L. A., Torres D. F., McCauley T. P., Romero G. E., Aharonian F. A., 2003, *ApJ*, 589, 481
 Archibald A. M., et al., 2009, *Science*, 324, 1411
 Archibald A. M., Kaspi V. M., Bogdanov S., Hessels J. W. T., Stairs I. H., Ransom S. M., McLaughlin M. A., 2010, *ApJ*, 722, 88

Becker W., 2009, in Becker W., ed., *Astrophysics and Space Science Library Vol. 357 of Astrophysics and Space Science Library, X-Ray Emission from Pulsars and Neutron Stars*. p. 91
 Bednarek W., 1993, *A&A*, 278, 307
 Bednarek W., 2009a, *A&A*, 495, 919
 Bednarek W., 2009b, *MNRAS*, 397, 1420
 Bhattacharya D., van den Heuvel E. P. J., 1991, *Phys.Rep.*, 203, 1
 Blumenthal G. R., Gould R. J., 1970, *Reviews of Modern Physics*, 42, 237
 Bogdanov S., Archibald A. M., Hessels J. W. T., Kaspi V. M., Lorimer D., McLaughlin M. A., Ransom S. M., Stairs I. H., 2011, *ApJ*, 742, 97
 Bogdanov S., et al., 2011, *ApJ*, 730, 81
 Butters O. W., Norton A. J., Hakala P., Mukai K., Barlow E. J., 2008, *A&A*, 487, 271
 Cheng K. S., Ruderman M., 1989, *ApJ*, 337, L77
 Coriat M., Fender R. P., Dubus G., 2012, *MNRAS*, 424, 1991
 Cusumano G., et al., 2003, *A&A*, 410, L9
 Cusumano G., et al., 2010, *A&A*, 524, A64
 D’Angelo C. R., Spruit H. C., 2010, *MNRAS*, 406, 1208
 D’Angelo C. R., Spruit H. C., 2011, *MNRAS*, 416, 893
 D’Angelo C. R., Spruit H. C., 2012, *MNRAS*, 420, 416
 de Cea del Pozo E., Torres D. F., Rodriguez Marrero A. Y., 2009, *ApJ*, 698, 1054
 De Martino D., et al., 2010, *A&A*, 515, A25
 De Martino D., et al., 2013, *A&A*, 550, A89
 Ekşi K. Y., Hernquist L., Narayan R., 2005, *ApJ*, 623, L41
 Fermi LAT Collaboration et al., 2009, *Science*, 326, 1512
 Frank J., King A., Raine D. J., 2002, *Accretion Power in Astrophysics: Third Edition*
 Frankel N. E., Hines K. C., Dewar R. L., 1979, *Phys. Rev. A*, 20, 2120
 Gallo E., Fender R. P., Pooley G. G., 2003, *MNRAS*, 344, 60
 Ghosh P., 2007, *Rotation and Accretion Powered Pulsars*. World Scientific Publishing Co
 Gierliński M., Zdziarski A. A., Poutanen J., Coppi P. S., Ebisawa K., Johnson W. N., 1999, *MNRAS*, 309, 496
 Halpern J. P., Gaidos E., Sheffield A., Price-Whelan A. M., Bogdanov S., 2013, *The Astronomer’s Telegram*, 5514, 1
 Hill A. B., et al., 2011, *MNRAS*, 415, 235
 Illarionov A. F., Sunyaev R. A., 1975, *A&A*, 39, 185
 in’t Zand J. J. M., Jonker P. G., Markwardt C. B., 2007, *A&A*, 465, 953
 Khangulyan D., Hnatic S., Aharonian F., 2007, *APSS*, 309, 261
 Kong A. K. H., 2013, *The Astronomer’s Telegram*, 5515, 1
 Kong A. K. H., Charles P. A., Kuulkers E., 1998, *NA*, 3, 301
 Lefa E., Kelner S. R., Aharonian F. A., 2012, *ApJ*, 753, 176
 Li J., Torres D. F., Zhang S., Papitto A., Chen Y., Wang J.-M., 2012, *ApJ*, 761, 49
 Lipunov V. M., Börner G., Wadhwa R. S., 1992, *Astrophysics of Neutron Stars*
 Lomb N. R., 1976, *APSS*, 39, 447
 Lovelace R. V. E., Romanova M. M., Bisnovatyi-Kogan G. S., 1995, *MNRAS*, 275, 244
 Malyshev D., Zdziarski A. A., Chernyakova M., 2013, *MNRAS*, 434, 2380
 Martín J., Torres D. F., Rea N., 2012, *MNRAS*, 427, 415
 Maselli A., Cusumano G., Massaro E., Segreto A., La Parola V., Tramacere A., Donnarumma I., 2011, *A&A*, 531, A153
 Masetti N., et al., 2006, *A&A*, 459, 21
 Migliari S., Fender R. P., 2006, *MNRAS*, 366, 79

- Papitto A., Bozzo E., Ferrigno C., Rea N., 2013, The Astronomer's Telegram, 5534, 1
- Papitto A., Ferrigno C., Bozzo E., Rea N., Pavan L., et al., 2013, Nat., 501, 517
- Papitto A., Torres D. F., Rea N., 2012, ApJ, 756, 188
- Patruno A., D'Angelo C., 2013, ApJ, 771, 94
- Patruno A., et al., 2013, arXiv:1310.7549
- Patruno A., Watts A., Klein Wolt M., Wijnands R., van der Klis M., 2009, ApJ, 707, 1296
- Patruno A., Watts A. L., 2012, arXiv:1206.2727
- Perna R., Bozzo E., Stella L., 2006, ApJ, 639, 363
- Press W. H., Flannery B. P., Teukolsky S. A., Vetterling W. T., 1989, Numerical recipes in C. The art of scientific computing
- Pretorius M. L., 2009, MNRAS, 395, 386
- Romanova M. M., Toropina O. D., Toropin Y. M., Lovelace R. V. E., 2003, ApJ, 588, 400
- Romanova M. M., Ustyugova G. V., Koldoba A. V., Lovelace R. V. E., 2009, MNRAS, 399, 1802
- Romero G. E., Kaufman Bernadó M. M., Combi J. A., Torres D. F., 2001, A&A, 376, 599
- Ruderman M., Shaham J., Tavani M., 1989, ApJ, 336, 507
- Rybicki G. B., Lightman A. P., 1979, Radiative processes in astrophysics
- Saitou K., Tsujimoto M., Ebisawa K., Ishida M., 2009, PASJ, 61, L13
- Sari R., Esin A. A., 2001, ApJ, 548, 787
- Scargle J. D., 1982, ApJ, 263, 835
- Sguera V., Drave S. P., Bird A. J., Bazzano A., Landi R., Ubertini P., 2011, MNRAS, 417, 573
- Spruit H. C., Taam R. E., 1993, ApJ, 402, 593
- Stappers B. W., et al., 2013, arXiv:1311.7506
- Syunyaev R. A., Shakura N. I., 1977, Soviet Astronomy Letters, 3, 138
- Tam P. H. T., et al., 2010, ApJ, 724, L207
- Tavani M., et al., 2009, Nat., 462, 620
- Torres D. F., 2004, ApJ, 617, 966
- Torres D. F., Rea N., Esposito P., et al., 2012, ApJ, 744, 106
- Ubertini P., Sguera V., Stephen J. B., Bassani L., Bazzano A., Bird A. J., 2009, ApJ, 706, L7
- Ustyugova G. V., Koldoba A. V., Romanova M. M., Lovelace R. V. E., 2006, ApJ, 646, 304
- Wang Y.-M., 1996, ApJ, 465, L111
- Wang Z., Archibald A. M., Thorstensen J. R., Kaspi V. M., Lorimer D. R., Stairs I., Ransom S. M., 2009, ApJ, 703, 2017
- Webb N. A., Olive J.-F., Barret D., 2004, A&A, 417, 181
- Winkler C., et al., 2003, A&A, 411, L1